Investigation of Factors Determining the Enhanced Permeability and Retention Effect in Subcutaneous Xenografts

Michiel Bolkestein[1], Erik de Blois[2], Stuart J. Koelewijn[2], Alexander M.M. Eggermont[3], Frank Grosveld[4], Marion de Jong[2], and Gerben A. Koning[1]

[1]Laboratory of Experimental Surgical Oncology, Department of Surgery, Erasmus MC, Rotterdam, The Netherlands; [2]Departments of Nuclear Medicine and Radiology, Erasmus MC, Rotterdam, The Netherlands; [3]Gustave Roussy Cancer Campus Grand Paris, Villejuif Paris, France; and [4]Department of Cell Biology, Erasmus MC, Rotterdam, The Netherlands

Liposomal chemotherapy offers several advantages over conventional therapies, including high intratumoral drug delivery, reduced side effects, prolonged circulation time, and the possibility to dose higher. The efficient delivery of liposomal chemotherapeutics relies, however, on the enhanced permeability and retention (EPR) effect, which refers to the ability of macromolecules to extravasate leaky tumor vessels and accumulate in the tumor tissue. Using a panel of human xenograft tumors, we evaluated the influence of the EPR effect on liposomal distribution in vivo by injection of pegylated liposomes radiolabeled with ^{111}In. Liposomal accumulation in tumors and organs was followed over time by SPECT/CT imaging. We observed that fast-growing xenografts, which may be less representative of tumor development in patients, showed higher liposomal accumulation than slow-growing xenografts. Additionally, several other parameters known to influence the EPR effect were evaluated, such as blood and lymphatic vessel density, intratumoral hypoxia, and the presence of infiltrating macrophages. The investigation of various parameters showed a few correlations. Although hypoxia, proliferation, and macrophage presence were associated with tumor growth, no hard conclusions or predictions could be made regarding the EPR effect or liposomal uptake. However, liposomal uptake was significantly correlated with tumor growth, with fast-growing tumors showing a higher uptake, although no biological determinants could be elucidated to explain this correlation.

Key Words: EPR effect; liposomes; SPECT; nanomedicine

J Nucl Med 2016; 57:601–607
DOI: 10.2967/jnumed.115.166173

Almost all nanocarriers, including liposomes (*1*), and many other anticancer drugs rely on the enhanced permeability and retention (EPR) effect for accumulation in tumor tissue. The EPR effect is defined as the process of extravasation of large molecules from leaky tumor vasculature, leading to accumulation in tumor tissue (*2*). The EPR effect is dependent on many biological parameters, with the development of the abnormal tumor vasculature playing a major role, although other parameters such as the composition of the surrounding stroma, absence of functional lymphatics, and presence of tumor infiltrating macrophages also play an important role (*3*). Abnormally upregulated growth factors affect the vasculature of the tumor (*4*) and lead to large endothelial junctions at the luminal surface, resulting in a leaky vasculature (*5*). In addition, vessels lack smooth muscle cell layers and supporting cells (*6*), and the fast recruitment of blood vessels results in tumor neovasculature that is not hierarchically organized, causing a heterogeneous spatial distribution (*4,7,8*). Finally, tumors overexpress many permeability-enhancing factors, which contribute to an enhanced EPR effect (*9*). These observations suggest that most tumors may be susceptible to nanoparticle treatment, but thus far such particles show only a limited effect in vivo due to various barriers such as the mononuclear phagocyte system, extracellular matrix, low pH, low oxygenation, and high interstitial fluid pressure (*10–12*). The intra- and intertumoral heterogeneity are major factors influencing the EPR effect, especially in patients, where tumor growth and vessel development are slower (*13*).

The Food and Drug Administration–approved liposomal doxorubicin (Doxil or Caelyx; Janssen Products, LP) is one of the most successful nanoparticle drugs for several cancer types (*14–17*). Unfortunately, Doxil has a limited effect on overall survival when compared with conventional chemotherapy (*3*), as has been shown in various clinical trials (*17–19*). This and previous results suggest that tumor physiology influences the efficacy of nanoparticle drugs, possibly due to variations in the EPR effect (*20*).

Because the EPR effect is essential for the efficacy and mode of action of liposomes in vivo, the aim of this study was to investigate major parameters influencing EPR and their effects on liposomal uptake in tumor xenografts. To this end, we injected unloaded, long-circulating, pegylated Doxil-like liposomes to determine liposomal tumor accumulation. Various human xenograft tumor models, including squamous cell carcinoma, breast cancer, and pancreatic cancer, were selected on the basis of tumor growth rate, taking into consideration that slow-growing tumors are more representative of tumor growth in patients. Our results show that it is difficult to elucidate single determinants of the EPR effect and we therefore suggest that liposomal uptake and distribution in tumors is a multifactorial process involving various physiological and morphological parameters.

MATERIALS AND METHODS

Preparation of Unloaded Doxil Liposomes

Unloaded Doxil-like liposomes were prepared as described in the supplemental information (supplemental materials are available at http://jnm.snmjournals.org).

Received Aug. 31, 2015; revision accepted Nov. 25, 2015.
For correspondence or reprints contact: Michiel Bolkestein, Laboratory of Experimental Surgical Oncology, Department of Surgery, Erasmus MC, Ee-175, P.O. Box 1738, 3000 DR Rotterdam, The Netherlands.
E-mail: m.bolkestein@erasmusmc.nl
Published online Dec. 30, 2015.

Cell Lines

All cell lines were obtained from the American Type Culture Collection and routinely cultured as described in the supplemental information.

^{111}In Labeling of Liposomes

Liposomes contained 0.1 mol% 1,2-distearoyl-sn-glycero-3-phosphoethanolamine-*N*-diethylenetriaminepentaacetic acid (DTPA-PE) lipid (Avanti Polar Lipids, Inc.), which enabled conjugation with ^{111}InCl (Mallinckrodt Medical B.V.). Approximately 30 MBq of ^{111}In were incubated per μmol of liposomes for 15 min at room temperature; 2.5 M sodium acetate was used to set the pH at 5.0. Instant thin-layer chromatography silica gel (silica gel–coated paper [Varian Inc.]; 0.1 M sodium citrate, mobile phase) was performed to ascertain complete labeling (*21*). Because of the molar excess of DTPA lipid over ^{111}In, lipid labeling efficiencies of greater than 99% were achieved. Before injections, the volume was adjusted to 200 μL per μmol of liposomes with *N*-(2-hydroxyethyl)piperazine-*N*-(2-ethanesulfonic acid) (HEPES)–buffered saline (10 mM HEPES, 135 mM NaCl, pH 7.4).

In Vivo Biodistribution Studies

Tumor inoculation of NMRI *nu/nu* mice is described in the supplemental information.

Mice were injected intravenously (tail) with 1 μmol of liposomes labeled with ^{111}In. Immediately after injection, the animal was scanned (t = 0), using the following settings: SPECT (nanoSPECT/CT; Mediso Medical Imaging Systems) static scan with 20 projections, 60 s/projection, and a quality factor of 0.8. APT1 apertures were used with 1.4 mm diameter pinholes (FOV 24 + 16 mm). The following were the CT scan settings: 240 projections, 45 kVp tube voltage, and 500 ms exposure. The t = 0 scan was followed by scans at 4, 8, 12, and 24 h after injection. SPECT/CT analysis was performed using InVivoScope/VivoQuant software (inviCRO). Three-dimensional regions of interest were drawn over the heart (blood pool) and tumor to calculate uptake of ^{111}In liposomes at the selected time points, after which they were corrected for volume (%ID/cm^3). Representative figures were made with the same software after correction for ^{111}In decay.

Ex Vivo Biodistribution

Tumors and tissue samples (blood [cardiac puncture], heart, lung, liver, spleen, pancreas, kidney, stomach, duodenum, caecum, colon, tail, and muscle) were harvested and weighed. Radioactivity was determined with a γ-counter (Perkin Elmer), and liposomal accumulation was calculated as percentage injected dose per gram of tissue (%ID/g) and corrected for radioactive decay of ^{111}In (half-life, 2.81 d). The injected dose was calculated by measuring the syringe before and after injection.

Immunohistochemical Staining

After the final scan, pimonidazole (60 mg/kg of body weight) was injected intraperitoneally and allowed to circulate for 4 h before dissection of tumor and organs. Harvested tumors were snap-frozen in liquid nitrogen, and frozen tumor sections were used for immunohistochemical staining as described in the supplemental information. Sections were stained for blood vessels (CD31), pegylated liposomes (PEG), macrophages (CD11b), lymphatic vessels (LYVE-1), vessel integrity (collagen IV), and hypoxia (pimonidazole).

Tile scans of fluorescently stained tumor sections were acquired using an LSM 510 Meta confocal microscope (Carl Zeiss B.V.) with a Plan-Neofluar 10× objective. Quantifications were performed with ImageJ (National Institutes of Health), using manual thresholding (range, 0–255) for density analysis and a colocalization threshold tool to ascertain the ratio between PEG and CD31, and collagen IV and CD31. To avoid regional bias, all quantifications were performed on whole tile scans of tumor sections.

Statistical Analysis

Statistical analyses were performed using GraphPad Prism (version 5.01; GraphPad Software). The differences between fast-, intermediate-, and slow-growing xenografts were evaluated using 1-way ANOVA with nonparametric Kruskal–Wallis *H* test and Dunn's multiple comparison post-test. Comparisons between the high- and low-uptake groups were performed using the 2-tailed Mann–Whitney *U* test. Correlation analysis between the various parameters evaluated in this study was performed using the Spearman *rho* test. All statistical tests were 2-sided, and a *P* value of lower than 0.05 was considered statistically significant.

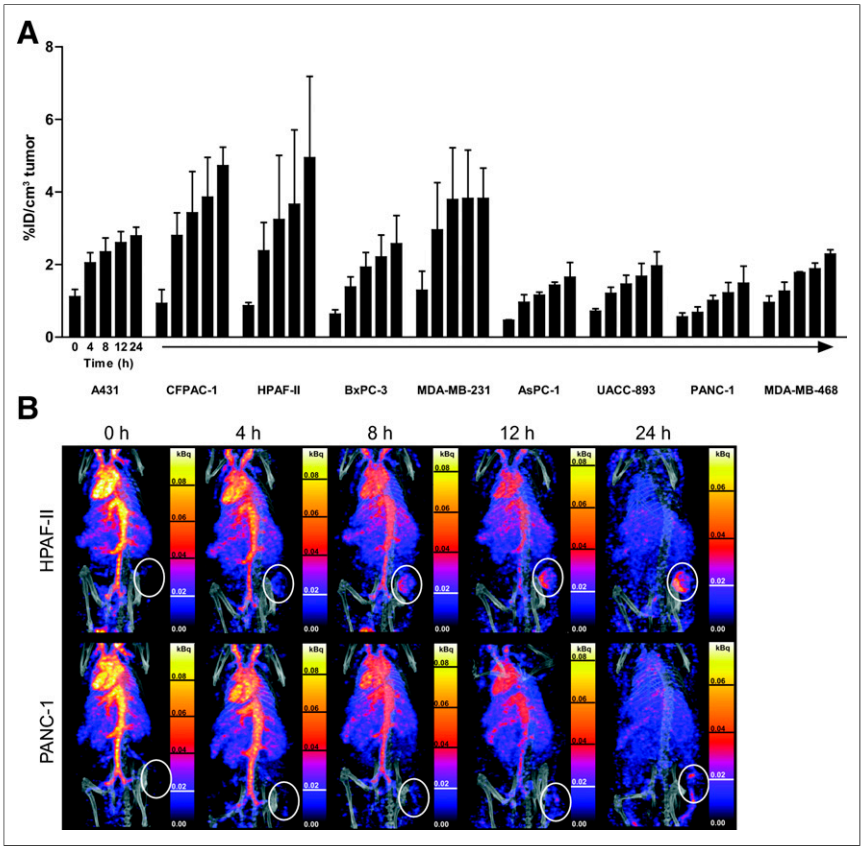

FIGURE 1. (A) Average tumor uptake in %ID/cm^3 was calculated and is depicted at 0, 4, 8, 12, and 24 h after injection. (B) Representative SPECT/CT scans, adjusted for ^{111}In half-life, of HPAF-II or PANC-1 tumor (white circle)–bearing mice at different time intervals after injection with ^{111}In-labeled liposomes, showing uptake of liposomes over time to a higher (HPAF-II) and lesser (PANC-1) degree.

RESULTS

Characterization of Liposomes

Liposomal characteristics, such as size and polydispersity, were confirmed to be similar to Doxil and are described in detail in the supplemental information.

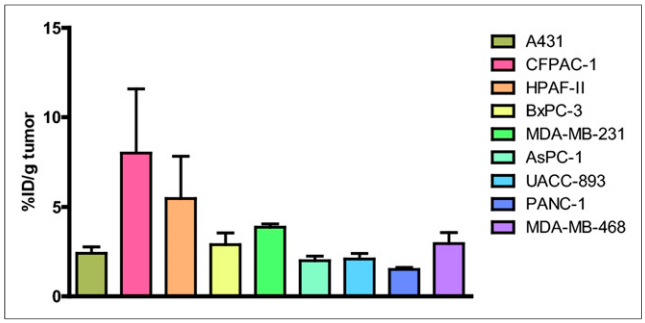

FIGURE 2. Tumor liposome accumulation of ^{111}In in %ID/g at 24 h after intravenous injection, ordered from fast- to slow-growing tumor xenografts.

To perform image-guided delivery, the liposomes were labeled with ^{111}In for SPECT imaging. The radiolabeling efficiency with ^{111}In after 15 min labeling at room temperature was greater than 99%. The ^{111}In-conjugated liposomes were tested for stability for up to 96 h as shown in Supplemental Figure 1. On average the liposomes were labeled with 34.54 ± 1.04 MBq of ^{111}In per μmol of liposomes.

Tumor Characterization

The supplemental information and Supplemental Figure 2 show the subdivision of tumor types based on growth rate.

In Vivo Localization of ^{111}In-Labeled Liposomes in Human Tumor Xenografts

All mice were injected intravenously with 1 μmol of liposomes labeled with ^{111}In for SPECT imaging. A volume of interest was drawn to quantify liposomal accumulation in the tumor and heart (blood pool). Figure 1A shows accumulation of liposomes in the tumor over time (0, 4, 8, 12, and 24 h after injection) as a percentage injected dose corrected for tumor volume (%ID/cm^3). The EPR effect ensured accumulation of liposomes in the tumors over time, whereas the heart showed clearance of liposomes from circulation. In the heart, liposomes still accounted for 6.28 ± 1.50 %ID/cm^3 (SD) after 24 h, which was confirmed by $t_{1/2}(\beta)$ of 16.99 ± 1.81 h (SEM). Figure 1B shows representative mice depicting high liposomal uptake (HPAF-II tumor) and low liposomal uptake (PANC-1 tumor). The SPECT/CT scans show radiolabeled liposomes in circulation, visible in the heart, aortic arch, aorta, and continuing downstream into axillary, hepatic, splenic, renal, and femoral arteries. The liposomes in circulation diminished over time and accumulated in the liver, spleen, and, to varying degrees, the tumor. The liposomes were slowly cleared via the liver and spleen (mononuclear phagocytic system), whereas they were retained in the tumor because of the EPR effect (*22*). Spleen macrophages and hepatic Kupfer cells can ingest liposomes and are responsible for liposome accumulation in these organs. Liver fenestrations (100 nm) and spleen lumina (up to 5 μm) will further contribute to this accumulation (*23*).

Supplemental Figure 3 shows all studied tumor types 12 h after injection with radiolabeled liposomes. In addition to differences in total uptake, early variations in intratumoral localization were clearly visible and were probably caused by perfusion differences (*24,25*). For example, MDA-MB-231 showed a clear uptake in certain regions of the tumor periphery, whereas other regions remained clear. Other tumors such as CFPAC-1 showed a more homogeneous distribution of liposomes. Importantly, the circulation of liposomes and accumulation in liver and spleen were comparable between different tumor models, as confirmed later by the biodistribution data. Liposomes are degraded in the liver after 12–24 h, causing a release of free ^{111}In-DTPA, as detected by low levels of radioactivity in the kidney and bladder, because free ^{111}In-DTPA is rapidly cleared from circulation (*26*).

Ex Vivo Organ Biodistribution

Radioactivity uptake was measured after resection of the tumors and other relevant tissues and is shown per tumor type in Figure 2 and in more detail for all analyzed organs, including the tumor, in Supplemental Figure 4. The tumors are again arranged from fast- to slow-growing, with levels of uptake ranging from PANC-1 (1.51 ± 0.11 %ID/g) on the low end to CFPAC-1 (7.99 ± 3.59 %ID/g) on the

TABLE 1
Comparison of Liposomal Uptake, Tumor Growth, and Morphology in High- Versus Low-Uptake Tumors

Characteristic	High uptake (n = 9)	Low uptake (n = 17)	P
Liposomal uptake			
Liposomes (in vivo)	4.16 (3.67–5.01)	2.12 (1.50–2.45)	<0.0001*
Liposomes (ex vivo)	4.24 (3.95–7.06)	2.26 (1.76–2.62)	<0.0001*
Time in days	25 (21–43)	70 (52–79)	0.0104*
Morphological parameters			
PEG percentage	5.64 (4.92–11.77)	2.50 (0.97–4.07)	0.0018*
CD31 percentage	2.84 (2.08–3.98)	2.87 (2.12–5.57)	0.5899
Pimonidazole percentage	37.13 (24.12–40.72)	33.49 (27.23–45.19)	0.6276
Ki-67 percentage	7.63 (5.32–9.21)	7.79 (5.52–11.39)	0.4188
LYVE-1 percentage	0.37 (0.15–0.79)	0.21 (0.06–0.41)	0.2465
CD11b percentage	1.01 (0.31–2.26)	1.40 (0.39–2.53)	0.4834
Collagen percentage	18.56 (12.23–20.23)	13.72 (8.31–16.46)	0.0524

*Significant at P level of less than 0.05.
Statistical test used was 2-tailed Mann–Whitney U test. Data are median, with interquartile ranges in parentheses.

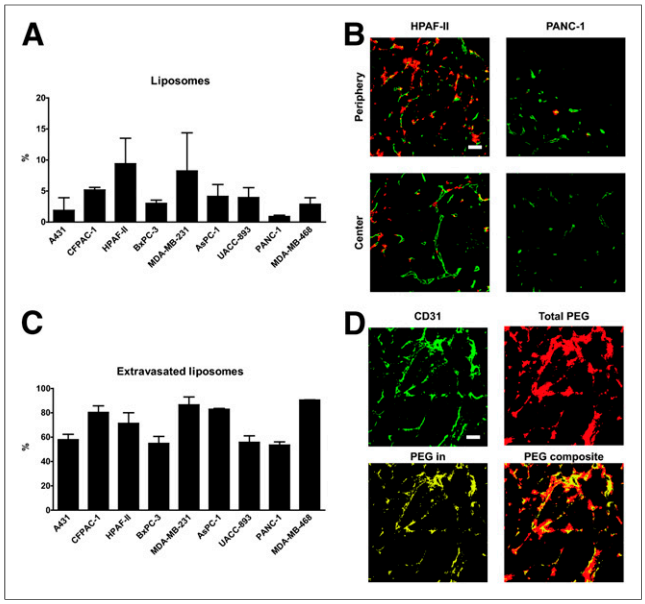

FIGURE 3. (A) Percentage of liposomal uptake calculated from immunohistochemical staining of PEG, which shows comparable uptake to in vivo/ex vivo quantifications. (B) Representative images of tumor periphery and center indicate that uptake in periphery is higher in both high- and low-uptake tumors. (C and D) Extravasated liposomes calculated for all tumors based on total PEG (red) minus PEG colocalized (yellow) with blood vessels (CD31, green), leading to final composite figure showing colocalized (yellow) and extravasated (red) liposomes. Degree of extravasation is relatively high in all tumors. All quantifications were performed on whole tile scans of tumor sections. Scale bars = 100 μm.

high end. A trend was observed between tumor growth and liposomal uptake (Table 1, $P = 0.0104$), although outliers, such as A431, BxPC-3, and MDA-MB-468, indicate that other factors are important and may be influencing liposomal accumulation. The reason for this was investigated in more detail using immunohistochemical stainings, but it is, for example, known that the presence of necrotic or poorly vascularized tumor cores in fast-growing tumors may inhibit liposomal uptake (*27*). Most of the liposomes accumulate in the liver, spleen, and tumor, after which they are cleared. Biodistribution data up to 96 h after injection are shown in Supplemental Figure 5, showing clearance of liposomes from most organs. Liposomal uptake in vivo was compared with other modalities used to detect liposomal uptake and the morphological parameters thought to influence the EPR effect and nanoparticle accumulation. To this end, the tumors were subdivided into high- and low-uptake groups; the high-uptake group included CFPAC-1, HPAF-II, and MDA-MB-231 xenografts. Table 1 shows that the difference in uptake between these groups can be detected with all tested modalities: in vivo SPECT/CT imaging, ex vivo biodistribution, and the anti-PEG antibody staining (P value < 0.0001, < 0.0001, and $= 0.0018$, respectively). In addition, there was a significant difference in tumor growth, that is, the time required for the tumors to reach 200 mm^3 ($P = 0.0104$). We did not observe a statistically significant correlation with any other morphological parameter evaluated.

Immunohistochemistry

To further investigate the underlying mechanisms of the EPR effect and to find possible explanations for the observed variations in liposomal tumor uptake, several morphological parameters were investigated using immunohistochemistry (Table 1). In Figure 3A, the percentage of total tumor areas positive for liposomal content was calculated using an anti-PEG antibody. This shows a significant correlation with the in vivo and ex vivo quantifications (Supplemental Table 1; $P = 0.007$ and < 0.001, respectively). Unfortunately, the aforementioned subdivision into slow-, intermediate-, and fast-growing xenografts did not result in significant correlations (Supplemental Table 2). Figure 3B shows HPAF-II and PANC-1 frames

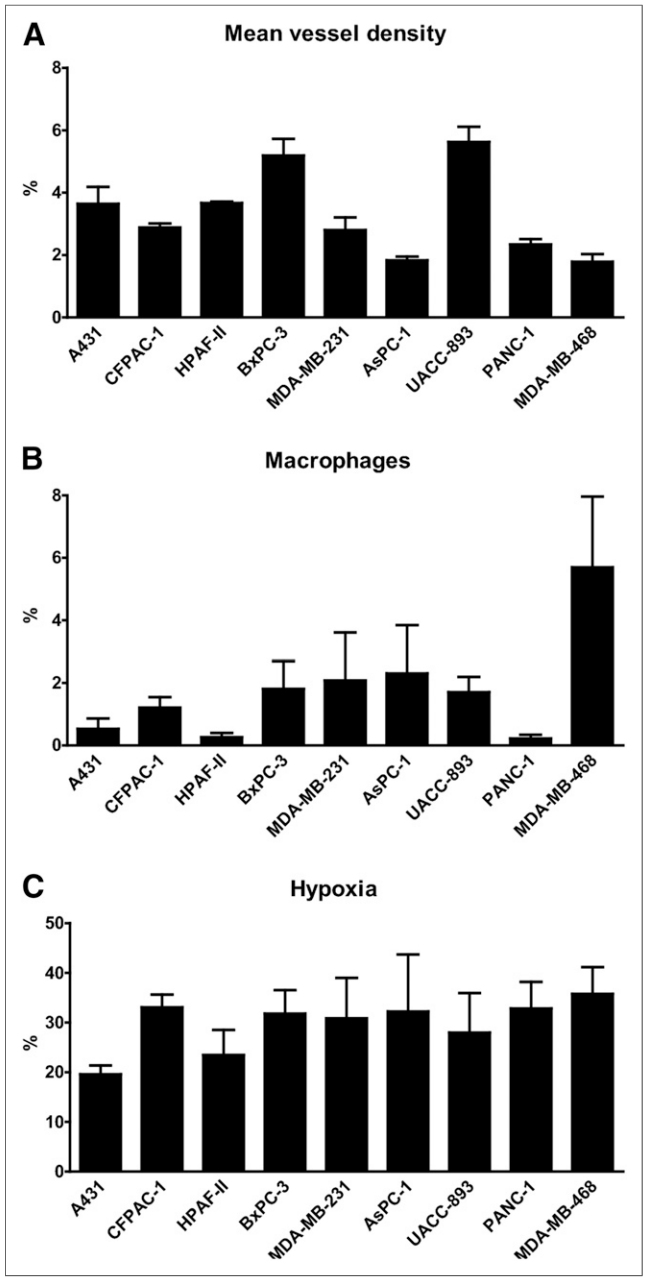

FIGURE 4. (A) Mean vessel density in tumors based on anti-CD31 staining. (B) Macrophages are stained with anti-CD11b antibody, and a high percentage is seen in MDA-MB-468 tumors. (C) Hypoxia percentage in different tumors, which was calculated on the basis of presence of pimonidazole after intraperitoneal injection. Degree of hypoxia is comparable for all tumors. All quantifications were performed on whole tile scans of tumor sections.

to demonstrate the difference of liposome localization in tumors with high and low uptake, respectively. Additionally, the intratumoral localization of the liposomes was determined in relation to blood vessels (CD31) showing that most liposomes had indeed extravasated from the vessels (Fig. 3C), although the distance traveled from the vessels is minimal. The percentage of extravasated liposomes was calculated by subtracting the amount of CD31-colocalized liposomes from the total amount of liposomes present in the area. This is depicted in Figure 3D, in which an example is given of a CD31 staining (green), total PEG staining (red), and the calculated colocalized liposomes (PEG in yellow), which shows liposomes within and extravasated from these vessels (shown in PEG composite in yellow and red, respectively). Although nanoparticle distribution and accumulation is undeniably related to the presence of blood vessels (*28*), Figure 4A shows that the number of vessels (depicted in percentage mean vessel density) cannot be used to predict the degree of liposomal uptake. For example, AsPC-1 and UACC-893 have a similar uptake of liposomes, depicted with in vivo, ex vivo, and immunohistochemical quantifications, but the mean vessel density of UACC-893 is 3 times higher than that of AsPC-1. Representative scans of the aforementioned stainings are shown in Supplemental Figure 6. As mentioned before, the factors influencing the EPR effect and the uptake of liposomes are more complex. The mononuclear phagocytic system also has a major influence on the delivery of liposomes, although detection by the mononuclear phagocytic system may be reduced by pegylation (*29,30*). Monocytes internalize liposomes, after which the drug may be released, resulting in toxic effects to the monocytes. Figure 4B shows that the percentage of macrophages in the tumor tissue is in general relatively low, with the exception of MDA-MB-468 (5.70% ± 2.26%). This might explain why a slow-growing tumor (5 mo) with a poor mean vessel density (1.79% ± 0.42%) still has a considerable liposomal uptake (2.87% ± 1.05%). Hypoxia is usually correlated with poor vascularization and indicative of poor drug uptake. Because of unrestrained tumor growth, cells move beyond the distance over which oxygen can diffuse (~150 μm), and drugs targeting fast-dividing cells will usually be less effective (*31,32*). All tumors show a comparable degree of hypoxia (Fig. 4C), suggesting that this aspect plays a minor role in these tumor models. The functionality of both blood and lymphatic vessels is thought to be of great importance to the EPR effect and eventual uptake of macromolecules (*2*). We therefore incorporated a lymphatic marker (LYVE-1) and a collagen IV antibody to measure lymphatic vessel density and collagen IV support of blood vessels. The lymphatic vessels (Figs. 5A and 5B) are important for drainage of the tissue, and the result suggests that the high presence of these vessels caused lower accumulation in BxPC-3 tumors. The intermediate-growing BxPC-3 has a high lymphatic vessel density, 1.52% ± 0.86%, and a lymphatic–to–blood vessel ratio of 0.35 ± 0.11, with a well-developed mean vessel density, 5.19% ± 0.92%, and still showed a relatively poor liposomal accumulation. In addition, BxPC-3 tumor cells grew in tight clusters, which may be an additional factor contributing to the lower uptake, because the tissue is less permeable to liposomes. Most tumors have blood vessels supported with collagen IV matrix, apart from MDA-MB-468 tumors (Figs. 5C and 5D). To decipher possible associations between liposomal uptake and the various morphological parameters tested, we performed a correlation analysis (Supplemental Table 1). Although there was a significant correlation between the percentage PEG and the liposomal uptake in vivo, no further significant correlations related to other tested morphological parameters could be found. A multivariate analysis requiring a much larger dataset may in the future enable elucidation of multiple factors contributing to the EPR effect.

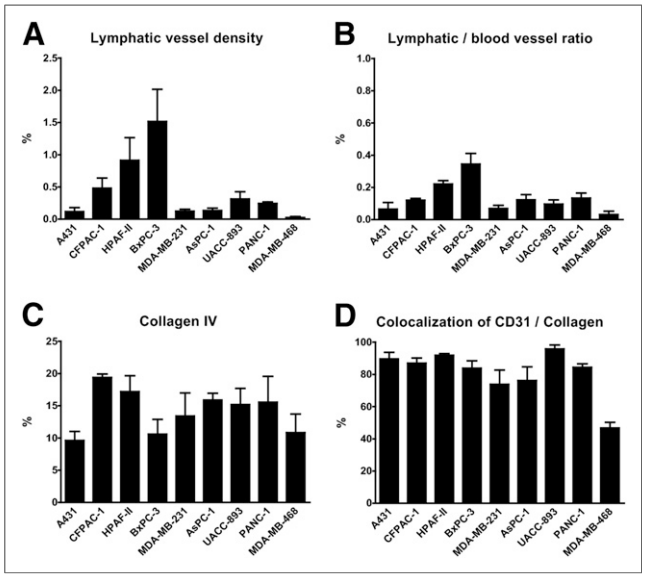

FIGURE 5. (A) LYVE-1 staining indicates presence of lymphatic vessels in the different tumors, which can be used to interpret possible drainage of tumor. (B) Lymphatic vessel (LYVE-1)–to–blood vessel (CD31) ratio is indicative of supply and drainage of tumor tissue. (C) Collagen IV is important for support of blood vessels and is used as a marker for mature blood vessels. Degree of collagen is comparable between tumors. (D) Colocalization of collagen IV and blood vessels (CD31) supports observation that most tumor vessels are mature and supported by collagen, with exception of MDA-MB-468. All quantifications were performed on whole tile scans of tumor sections.

DISCUSSION

The EPR effect, first described by Matsumura and Maeda in 1986 (*2*), shows tumor-specific accumulation of large molecules and is dependent on the following parameters: the size of the molecules should be larger than the renal clearance threshold (7 nm) to prevent fast clearance; the molecules should have characteristics that ensure a long circulation time to increase the chance for extravasation; and the nature of the tumor has to be such that it will ensure retention of these molecules, usually ranging from days to weeks, leading to enhanced efficacy. These properties distinguish the EPR effect needed for therapeutic purposes from targeting of low-molecular-weight molecules with a short half-life and fast clearance, which are more suited for imaging purposes (*33*). By utilizing the EPR effect, pegylated liposomes such as Doxil have been successful in the treatment of certain cancers.

This study has consolidated that pegylated liposomes can accumulate in various solid tumors, although considerable differences in uptake were observed. Uptake levels ranged from PANC-1 to CFPAC-1 at the low to high end, respectively. There was a trend between liposome accumulation and the speed of tumor growth. Although tumors, such as squamous cell carcinoma A431, showed very fast tumor growth but had limited liposomal accumulation in the tumor. This could be explained by the high growth rate and relatively large size of these tumors.

Angiogenesis is increased during tumor growth (*34*) and the tumor will grow exponentially until sufficient vascularization can no longer be sustained. This leads to hypoxic or necrotic tumor cores, which are more difficult to reach with anticancer drugs. Before this point is reached, the chaotic development of tumor vasculature together with the obstruction and collapse of lymphatic vessels at the tumor core will lead to an enhanced EPR effect and possibly an increased accumulation of nanoparticles (*2*). Lymphatic vessel density evaluation revealed that most tumors had an impaired lymphatic system aiding liposome accumulation. The exception was the intermediate-growing BxPC-3, which had a high lymphatic vessel density and a well-developed mean vessel density, resulting in a relatively poor liposomal accumulation. Although it has been hypothesized that normalization of the vasculature, extracellular matrix, and lymphatic vessels would lead to better delivery of drugs (*35*), this may not always hold true for liposomal drugs. Normalization of vessels will lead to a less leaky vasculature, which might impair the EPR effect.

It has also been shown that mean vessel density correlates with the degree of liposome accumulation (*28*), but we did not observe this correlation in our study. The liposomes were still in circulation after 24 h. Various degrees of colocalization of blood vessels and liposomes were observed, but most liposomes had extravasated from tumor vessels. Unfortunately, high levels of extravasation do not always result in high efficacy, due to the poor penetration characteristics of liposomes. The liposomes did not penetrate further than the perivascular space, confirming that smaller particles (12 nm) can penetrate a tumor heterogeneously up to 80 μm, but particles of 60 nm and larger do not leave the perivascular space or even the vessel (*36*). Several additional barriers such as high interstitial fluid pressure, low oxygenation, and the extracellular matrix need to be overcome (*12*).

Various other variables can influence the uptake of liposomes and the EPR effect in addition to the important role of the vasculature. For example, associated inflammation (*37*) and interactions with monocytes (*38*) can play a major role to increase the liposomal uptake in the tumor. This may explain why MDA-MB-468 had an intermediate liposomal uptake even though the mean vessel density was low. The monocyte staining to determine the involvement of the immune system showed a high presence of macrophages in MDA-MB-468 as opposed to the other tumors.

This study supports the notion that the EPR effect is a highly complex, multifactorial, heterogeneous phenomenon, which is possibly much larger in animal tumors than in human tumors (*13*). Because tumors are usually faster-growing in animal models, it is to be expected that they will have a higher degree of vascularization and a lesser developed vascular environment, leading to a high EPR effect. For this reason, we also investigated slow-growing tumors with a lower vessel density to explore pegylated liposomes in a more clinically relevant setting. Especially the pancreatic tumor models are more representative for the clinical setting, in which human tumors grow over long periods of time (*39*). Slow-growing tumors, such as prostate and pancreatic tumors, are known to have more normalized vessels and are usually difficult to treat with nanomedicine. Here, we showed that even within the pancreatic tumor models, there is a wide range in liposomal uptake and EPR effect, which accentuates the importance of selecting the appropriate tumor model for preclinical studies. In addition, it is crucial to include an imaging modality in studies investigating the effects of nanoparticle accumulation in vivo and to intervene if the therapy is inhibited by poor access to the tumor. Fortunately, an increasing number of methods to enhance the EPR effect in tumors have been developed, both in preclinical and clinical settings, including the use of heat to increase vessel permeability and induce extravasation of nanomedicine (*40–43*).

CONCLUSION

The EPR effect can be used to predict liposomal accumulation into tumors or explain limited uptake. In this study, we investigated several parameters and our results suggest that the EPR effect, and thus liposomal uptake, is a complex, multifactorial, and heterogeneous phenomenon. This is caused by tumor (microenvironment) variability, which therefore should be taken into account when considering liposomes as an anticancer therapy.

DISCLOSURE

The costs of publication of this article were defrayed in part by the payment of page charges. Therefore, and solely to indicate this fact, this article is hereby marked "advertisement" in accordance with 18 USC section 1734. No potential conflict of interest relevant to this article was reported.

ACKNOWLEDGMENTS

We thank Jan de Swart for technical support for the nanoSPECT/CT and Gert van Cappellen for advice on imaging and quantification of the immunohistochemical stainings.

REFERENCES

1. Bangham AD, Standish MM, Watkins JC. Diffusion of univalent ions across the lamellae of swollen phospholipids. *J Mol Biol.* 1965;13:238–252.
2. Matsumura Y, Maeda H. A new concept for macromolecular therapeutics in cancer chemotherapy: mechanism of tumoritropic accumulation of proteins and the antitumor agent smancs. *Cancer Res.* 1986;46:6387–6392.
3. Prabhakar U, Maeda H, Jain RK, et al. Challenges and key considerations of the enhanced permeability and retention effect for nanomedicine drug delivery in oncology. *Cancer Res.* 2013;73:2412–2417.
4. Jain RK, Stylianopoulos T. Delivering nanomedicine to solid tumors. *Nat Rev Clin Oncol.* 2010;7:653–664.
5. Jain RK. Transport of molecules across tumor vasculature. *Cancer Metastasis Rev.* 1987;6:559–593.
6. Konerding MA, Miodonski AJ, Lametschwandtner A. Microvascular corrosion casting in the study of tumor vascularity: a review. *Scanning Microsc.* 1995;9: 1233–1243.
7. Fang J, Nakamura H, Maeda H. The EPR effect: Unique features of tumor blood vessels for drug delivery, factors involved, and limitations and augmentation of the effect. *Adv Drug Deliv Rev.* 2011;63:136–151.
8. Dvorak HF, Nagy JA, Dvorak JT, Dvorak AM. Identification and characterization of the blood vessels of solid tumors that are leaky to circulating macromolecules. *Am J Pathol.* 1988;133:95–109.
9. Zhou Y, Kopecek J. Biological rationale for the design of polymeric anti-cancer nanomedicines. *J Drug Target.* 2013;21:1–26.
10. Fukumura D, Jain RK. Tumor microvasculature and microenvironment: targets for anti-angiogenesis and normalization. *Microvasc Res.* 2007;74:72–84.
11. Minchinton AI, Tannock IF. Drug penetration in solid tumours. *Nat Rev Cancer.* 2006;6:583–592.
12. Sriraman SK, Aryasomayajula B, Torchilin VP. Barriers to drug delivery in solid tumors. *Tissue Barriers.* 2014;2:e29528.
13. Lammers T, Kiessling F, Hennink WE, Storm G. Drug targeting to tumors: principles, pitfalls and (pre-) clinical progress. *J Control Release.* 2012;161: 175–187.
14. Ranson MR, Carmichael J, O'Byrne K, Stewart S, Smith D, Howell A. Treatment of advanced breast cancer with sterically stabilized liposomal doxorubicin: results of a multicenter phase II trial. *J Clin Oncol.* 1997;15: 3185–3191.

15. Muggia FM, Hainsworth JD, Jeffers S, et al. Phase II study of liposomal doxorubicin in refractory ovarian cancer: antitumor activity and toxicity modification by liposomal encapsulation. *J Clin Oncol.* 1997;15:987–993.
16. Stewart S, Jablonowski H, Goebel FD, et al. Randomized comparative trial of pegylated liposomal doxorubicin versus bleomycin and vincristine in the treatment of AIDS-related Kaposi's sarcoma. International Pegylated Liposomal Doxorubicin Study Group. *J Clin Oncol.* 1998;16:683–691.
17. Northfelt DW, Dezube BJ, Thommes JA, et al. Pegylated-liposomal doxorubicin versus doxorubicin, bleomycin, and vincristine in the treatment of AIDS-related Kaposi's sarcoma: results of a randomized phase III clinical trial. *J Clin Oncol.* 1998;16:2445–2451.
18. O'Brien ME, Wigler N, Inbar M, et al. Reduced cardiotoxicity and comparable efficacy in a phase III trial of pegylated liposomal doxorubicin HCl (CAELYX/Doxil) versus conventional doxorubicin for first-line treatment of metastatic breast cancer. *Ann Oncol.* 2004;15:440–449.
19. Gordon AN, Fleagle JT, Guthrie D, Parkin DE, Gore ME, Lacave AJ. Recurrent epithelial ovarian carcinoma: a randomized phase III study of pegylated liposomal doxorubicin versus topotecan. *J Clin Oncol.* 2001;19:3312–3322.
20. Harrington KJ, Mohammadtaghi S, Uster PS, et al. Effective targeting of solid tumors in patients with locally advanced cancers by radiolabeled pegylated liposomes. *Clin Cancer Res.* 2001;7:243–254.
21. Bakker WH, Albert R, Bruns C, et al. [^{111}In-DTPA-D-Phe1]-octreotide, a potential radiopharmaceutical for imaging of somatostatin receptor-positive tumors: synthesis, radiolabeling and *in vitro* validation. *Life Sci.* 1991;49:1583–1591.
22. Ishida T, Harashima H, Kiwada H. Liposome clearance. *Biosci Rep.* 2002;22:197–224.
23. Sarin H. Physiologic upper limits of pore size of different blood capillary types and another perspective on the dual pore theory of microvascular permeability. *J Angiogenes Res.* 2010;2:14.
24. Toy R, Hayden E, Camann A, et al. Multimodal *in vivo* imaging exposes the voyage of nanoparticles in tumor microcirculation. *ACS Nano.* 2013;7:3118–3129.
25. Bol K, Haeck JC, Groen HC, et al. Can DCE-MRI explain the heterogeneity in radiopeptide uptake imaged by SPECT in a pancreatic neuroendocrine tumor model? *PLoS One.* 2013;8:e77076.
26. Harrington KJ, Rowlinson-Busza G, Syrigos KN, Uster PS, Abra RM, Stewart JS. Biodistribution and pharmacokinetics of ^{111}In-DTPA-labelled pegylated liposomes in a human tumour xenograft model: implications for novel targeting strategies. *Br J Cancer.* 2000;83:232–238.
27. Harrington KJ, Rowlinson-Busza G, Syrigos KN, et al. Influence of tumour size on uptake of ^{111}In-DTPA-labelled pegylated liposomes in a human tumour xenograft model. *Br J Cancer.* 2000;83:684–688.
28. Koukourakis MI, Koukouraki S, Giatromanolaki A, et al. Liposomal doxorubicin and conventionally fractionated radiotherapy in the treatment of locally advanced non-small-cell lung cancer and head and neck cancer. *J Clin Oncol.* 1999;17:3512–3521.
29. Papahadjopoulos D, Allen TM, Gabizon A, et al. Sterically stabilized liposomes: improvements in pharmacokinetics and antitumor therapeutic efficacy. *Proc Natl Acad Sci USA.* 1991;88:11460–11464.
30. Gabizon A, Shmeeda H, Barenholz Y. Pharmacokinetics of pegylated liposomal Doxorubicin: review of animal and human studies. *Clin Pharmacokinet.* 2003;42:419–436.
31. Brown JM, Giaccia AJ. The unique physiology of solid tumors: opportunities (and problems) for cancer therapy. *Cancer Res.* 1998;58:1408–1416.
32. Durand RE. The influence of microenvironmental factors during cancer therapy. *In Vivo.* 1994;8:691–702.
33. Maeda H. Vascular permeability in cancer and infection as related to macromolecular drug delivery, with emphasis on the EPR effect for tumor-selective drug targeting. *Proc Jpn Acad, Ser B, Phys Biol Sci.* 2012;88:53–71.
34. Folkman J. Angiogenesis in cancer, vascular, rheumatoid and other disease. *Nat Med.* 1995;1:27–31.
35. Jain RK. Normalizing tumor microenvironment to treat cancer: bench to bedside to biomarkers. *J Clin Oncol.* 2013;31:2205–2218.
36. Popović Z, Liu W, Chauhan VP, et al. A nanoparticle size series for *in vivo* fluorescence imaging. *Angew Chem Int Ed Engl.* 2010;49:8649–8652.
37. Boerman OC, Storm G, Oyen WJ, et al. Sterically stabilized liposomes labeled with indium-111 to image focal infection. *J Nucl Med.* 1995;36:1639–1644.
38. Caron WP, Song G, Kumar P, Rawal S, Zamboni WC. Interpatient pharmacokinetic and pharmacodynamic variability of carrier-mediated anticancer agents. *Clin Pharmacol Ther.* 2012;91:802–812.
39. Furukawa H, Iwata R, Moriyama N. Growth rate of pancreatic adenocarcinoma: initial clinical experience. *Pancreas.* 2001;22:366–369.
40. Li L, Ten Hagen TL, Bolkestein M, et al. Improved intratumoral nanoparticle extravasation and penetration by mild hyperthermia. *J Control Release.* 2013;167:130–137.
41. Maeda H, Nakamura H, Fang J. The EPR effect for macromolecular drug delivery to solid tumors: Improvement of tumor uptake, lowering of systemic toxicity, and distinct tumor imaging *in vivo*. *Adv Drug Deliv Rev.* 2013;65:71–79.
42. Wong PP, Demircioglu F, Ghazaly E, et al. Dual-action combination therapy enhances angiogenesis while reducing tumor growth and spread. *Cancer Cell.* 2015;27:123–137.
43. Bridges E, Harris AL. Vascular-promoting therapy reduced tumor growth and progression by improving chemotherapy efficacy. *Cancer Cell.* 2015;27:7–9.